ACS Photonics 2023, 10, 3, 609–622
(doi: https://doi.org/10.1021/acsphotonics.2c01571)

Making Eu^{2+} and Sm^{2+} doped borates fit for solar energy applications

L.J.B. Erasmus[1,2], P.F. Smet[2], R.E. Kroon[1], D. Poelman[2], J.J. Terblans[1], J.J. Joos[2], D. Van der Heggen[2], H.C. Swart[1]

[1]Department of Physics, University of the Free State, Bloemfontein, South Africa

[2]Department of Solid State Sciences, Ghent University, Ghent, Belgium

Corresponding author e-mail address: erasmuslb@ufs.ac.za

Abstract:

Despite the development of many luminescent materials for various applications, only a few of these phosphors are applicable for solar energy generation applications. This study used the conventional solid-state reaction method to synthesise different strontium borate compounds co-doped with divalent europium and samarium ions. The material was optimised by varying the experimental procedure, the molar ratio of the boron and the molar ratios of both co-dopants. Strontium hexaborate doped with a relatively high europium concentration and a low samarium concentration ($Sr_{0.89}B_6O_{10}$:$Eu_{0.1}$, $Sm_{0.01}$) gave the optimum optical properties. These properties included a broad excitation range from 220 nm to 600 nm containing contributions from divalent europium and samarium ions. The material exhibited strong and narrow emission in the region from 650 nm to 850 nm following radiative transitions within the divalent samarium ions. The internal luminescence quantum efficiency of the optimised material was 79% (λ_{ex} = 508.5 nm). There was no spectral overlap between the excitation and emission spectra, thereby reducing the reabsorption probability. These marked characteristics make this phosphor material appropriate for use as a solar radiation converter or for use in luminescent solar concentrators.

Keywords:

Strontium borate, rare-earth ions, downshifting phosphor materials, solar application, luminescent solar concentrators

Introduction

One of the factors that fundamentally hampers solar cell efficiency is thermalisation loss from short-wavelength photons. This problem stems from the fact that the standard solar spectrum peaks at about

530 nm (1) while, for silicon and gallium arsenide solar cells, the highest solar cell spectral response is achieved at about 820 nm (2) and 700 nm (3), respectively. The spectral mismatch between the solar spectrum and the absorption spectrum of solar cells results in lower efficiencies (4). Numerous studies have investigated the use of downshifting phosphor materials to aid solar cells in this regard as demonstrated in references (4), (5) and (6). A phosphor material usually consists of a host material doped with rare-earth ions (7). Ideally, the rare-earth ions absorb a wide range of the short wavelengths of solar radiation and convert it to longer wavelengths of light for absorption by a solar cell.

The application field of luminescent solar concentrators (LSC) is also of specific interest for these phosphor materials. An LSC consists of a transparent waveguide with embedded luminescent material. The large area of the waveguide collects a portion of the solar radiation. This solar radiation is then absorbed and downshifted to longer wavelengths by the embedded phosphor particles. There should be little to no spectral overlap between the absorption and emission of the phosphor material to allow propagation of the emitted light over a long distance in the waveguide without absorption and re-direction upon re-emission. Most of the emitted light is directed by internal reflection in the waveguide towards smaller areas on the sides. Strategically placed solar cells on the waveguide edges are then used to convert the concentrated light to electricity. Hence a large collection area can be coupled to a limited solar cell area as shown in the studies referenced in (5), (6) and (8). Since only small solar cells are needed at the sides, high efficiency (and expensive per unit area) solar cells can be used.

Rare-earth ions that show promise for solar application are the divalent europium (Eu^{2+}) ion used in conjunction with the divalent samarium (Sm^{2+}) ion (5). In this case, the Eu^{2+} ion is used as a sensitiser, while the Sm^{2+} ion is the activator ion. This study aims to identify a suitable host for these ions and, by empirical methods, optimise the phosphor material for application in solar technology.

Theory and Literature Review

Dopant Ions

Figure 1 shows a) the partial energy level diagrams for Eu^{2+} and Sm^{2+} ions and b) the resulting excitation and emission spectra. The electronic structure of Sm^{2+} ions has a relatively low $4f^55d^1$ excited electronic configuration, resulting in significant overlap with the ^5D_J levels of the $4f^6$ configuration (9). The energy position of the broad $4f^6$ - $4f^55d^1$ excitation band of the Sm^{2+} ions can be influenced by the chemical environment of the ion (10) which is determined by covalency of the bonds, coordination number, crystal field strength and point symmetry (11). When a Sm^{2+} ion is optically excited to the $4f^55d^1$ manifold, it quickly decays non-radiatively to a lower $4f^6(^5D_0)$ level from where sharp intra-configurational $4f^6$ line emission can occur (12). These transitions are labelled $^5D_0$ - ^7F_J (J = 0-6), as

shown in Figure 1 b) (13). Some weak emission in the 620 - 650 nm range is shown in the inset in Figure 1 b). This emission originates from the higher $^5D_1$ level (14). The spectral details of these intra-configurational $4f^6$ emissions are only weakly sensitive to the chemical environment due to the filled 5s and 5p shells that shield the 4f electrons (15).

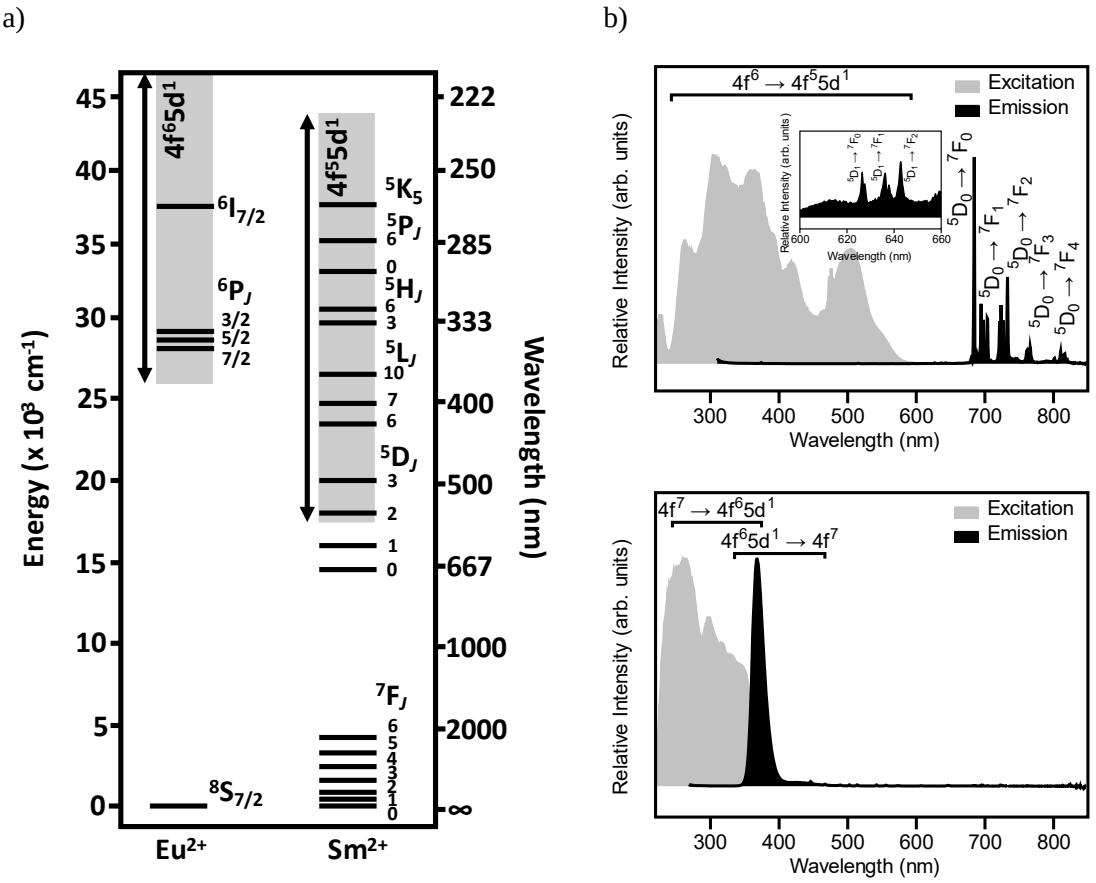

Figure 1: a) Partial energy diagram of divalent samarium and europium ions containing some of the $4f^N$ levels and showing the energy range of the low-energy part of the $4f^{N-1}5d^1$ manifolds. Different components of this figure are adapted from references (16) *and* (17)*. The figure includes a wavelength scale that is relevant only for the emissions that have the ground state as final state. b) Characteristic excitation and emission spectra for samarium (top) and europium (bottom) doped strontium borate compounds. Inset in the top figure shows weak emission from the higher $^5D_1$ level of the divalent samarium ion.*

Eu^{2+} ions have a relatively broad excitation band, and the emission bands are typically in the ultraviolet to the visible range, as shown in Figure 1b . These broad spectra are due to parity and spin allowed $4f^7$ - $4f^65d^1$ electric dipole transitions which overlap with the much weaker parity-forbidden intra-configurational $4f^7$ - $4f^7$ transitions (18). The position and splitting of the $4f^65d^1$ band are strongly dependent on the covalency, the size of the cation and the ligand field of the surrounding host material, leading to variations in the emission colour from the near-ultraviolet across the visible wavelength range (16). As shown in Figure 1b, Eu^{2+} doped strontium hexaborate has an excitation band that peaks at 264 nm while the emission band peaks at 385 nm.

Due to the allowed nature of the $4f^6 5d^1$ – $4f^7$ transitions, their transition probability $A_{tot}(\mathrm{Eu})$ is relatively high which results in radiative lifetimes which are in the τ = 0.2 µs to 2 µs range (19). The emission decay constant (in units of s) for the Eu^{2+} ions can be estimated by using Equation 1 (13). The value of χ contains all refraction-index dependent factors, resulting from the Einstein coefficient for spontaneous emission and local field effects and can be calculated using Equation 2, where n is the refractive index of the host material. The value of constant K is 5.06×10^{-8} $cm^3/Å^2s$. The value of radial integral $\langle 5d|r|4f\rangle$ is dependent on the chemical environment of the host material and usually a standard value of 0.81 Å is used while σ represents the energy of the emission band in units of cm^{-1} (19).

$$A_{tot}(\mathrm{Eu}) = \frac{1}{\tau} = K|\langle 5d|r|4f\rangle|^2 \chi \sigma^3$$

Equation 1

$$\chi = \frac{n(n^2+2)^2}{9}$$

Equation 2

Energy transfer can occur between nearby sensitiser and activator ions in a host crystal provided that their energy levels match, which is the case for Eu^{2+} and Sm^{2+}. In this case the Eu^{2+} ion is the sensitiser and Sm^{2+} ion is the activator ion. Energy transfer is characterised by a decrease in the sensitiser ion's luminescence intensity and a shortening of the decay as the concentration of activator ion is increased. The energy transfer efficiency, η_{ET} is given by Equation 3 where $\langle\tau_{sen}\rangle$ and $\langle\tau_{no\ sen}\rangle$ are the sensitiser ion's average decay constant with and without the activator ions present, respectively (20). The average decay constant is used, because when energy transfer occurs, the luminescence decay is no longer a simple exponential.

$$\eta_{ET} = 1 - \frac{\langle\tau_{sen}\rangle}{\langle\tau_{no\ sen}\rangle}$$

Equation 3

The spacing between the ions for optimum energy transfer can be expressed as the critical energy transfer distance. Reade's statistical model can be used in order to estimate this value (21). This model considers the luminescence quenching of the sensitiser ion with increasing concentration of the activator ion. The dependence of the normalised emission intensity of the sensitiser ion, $I_{sen}/I_{no\ sen}$ as a function of activator ion concentration, C_{act} is given by Equation 4. The resulting critical energy transfer volume $V_{crit(ET)}$ is used to determine the critical energy transfer distance, where it is implicitly assumed that dopants are stochastically distributed in the host crystal.

$$\frac{I_{sen}}{I_{no\ sen}} = \exp\left(-V_{crit(ET)}C_{act}\right)$$

Equation 4

Increasing the concentration of the activator or sensitiser ions can increase the absorption and lead to higher emission. However, if the concentration of the ions is too high, the probability for non-radiative release of energy increases, due to an increase in the energy migration between ions that can lead to energy loss through non-fluorescent ions or crystallographic defects (21). This effect leads to a decrease in emission intensity and is therefore known as concentration quenching (13). To quantify these effects, the critical distance between the ions $R_{crit(act/sen)}$ must be determined. This can be done by using Equation 5 where V_{Site} is the formal volume per possible crystallographic site for the activator ions, and $x_{crit(act/sen)}$ is the experimentally determined critical molar ratio for the respective ions (22).

$$R_{crit(act/sen)} \approx 2\left(\frac{3V_{Site}}{4\pi x_{crit(act/sen)}}\right)^{1/3}$$

Equation 5

Host Material

The next part to consider when synthesising a phosphor material is a suitable host material. One of the main functions of the host material is to stabilise the dopant ions. Strontium borate materials are viable due to their unique ability to stabilise some lanthanide dopants in a divalent oxidation state (23). Strontium borates are also of interest due to their wide bandgap (> 7 eV), ensuring little optical and electronic interference with the Eu^{2+} and Sm^{2+} ions. Therefore, over a wide energy range, the excitation and emission properties are driven by the dopant ions only.

The divalent strontium (Sr^{2+}) in strontium borates is substituted when doped with divalent ions (24). In order not to cause severe distortion in the structure, the difference in the crystal radii of the dopants must be less than 15% compared to the cation in the crystal structure that is replaced (10). Sr^{2+} ions have an ionic radius of 1.45 Å (Coordination number: 9). In comparison, Eu^{2+} and Sm^{2+} ions have ionic radii of 1.44 Å (Coordination number: 9) and 1.46 Å (Coordination number: 9) respectively, which is a sufficiently close match to incorporate the dopants on the Sr^{2+} crystallographic sites (25).

In previous studies (12), (24) it has been observed that the structure of the strontium borate host significantly influences the stability of the divalent dopant ions. This is due to the fact that the stability of the divalent dopant ions depends on the nature of the coordinating borate anions that surround them. According to a study by Pir et al. the stability of the dopant ions is influenced by the degree of balance of the formal charge on the surrounding oxygen atoms. That study postulates that the formal volume of

the oxygen sites in the lattice can be used as a quantitative measure for the degree of balance of the formal charge (24).

Therefore, the formal volume per oxygen atom V_O can be used to quantify the stability of different dopant oxidation states, where a lower formal volume results in a more stable host material for the divalent dopant ions (24). The formal volume per oxygen atom V_O is calculated using Equation 6, where V is the unit cell volume, Z is the number of formula units per unit cell and n_{atoms} is the number of atoms per formula unit of the specific structure. Table 1 gives these values together with the calculated formal volume per oxygen atom for the strontium metaborate (SrB_2O_4), strontium tetraborate (SrB_4O_7), strontium hexaborate (SrB_6O_{10}), and strontium octaborate (SrB_8O_{13}) structures. From the structures considered, both the SrB_4O_7 and SrB_6O_{10} systems show the most promise in stabilising the dopant ions in the divalent state.

$$V_O = \frac{V}{Zn_{atoms}}$$

Equation 6

Table 1: Unit cell parameters that is used for the calculation of formal volume per oxygen atom for a selection of strontium borate structures.

Host material	V **(Å^3)**	Z	n_{atoms}	$\boldsymbol{V_O}$ **(Å^3)**
SrB_4O_7	201	2	7	14.4
SrB_6O_{10}	575	4	10	14.4
SrB_8O_{13}	1931	8	13	18.6
SrB_2O_4	343	4	4	21.4

A possible process of incorporating trivalent dopant ions into these structures can be explained by a charge compensation mechanism which is described in the study by Zeng et al. (26) and illustrated in Figure S1-1 in the supporting information. As stated before, when dopant ions are introduced into strontium borates structures, they occupy the Sr^{2+} ion's crystallographic site. If the dopants ions are in the trivalent state, two trivalent ions are needed to substitute three Sr^{2+} sites to maintain the charge balance of the crystal. This results in the formation of a vacancy defect at one of the Sr^{2+} sites. Due to the absence of the Sr^{2+} ion this vacancy defect has two negative charges. These charges can be transferred to the trivalent dopant ions, which will result in the trivalent ions being reduced to the divalent state.

Experimental and Methodology

Synthesis

As explained in the Theory and Literature Review section, the SrB_4O_7 and SrB_6O_{10} structures are promising to stabilise the dopant ions into the divalent state. Therefore, this work focussed on the synthesis of these structures. Due to the application potential of the material in large area devices, the synthesis procedure must be scalable. Consequently, the high-temperature solid-state synthesis method used in a study by Jiayne et al. was investigated and used as starting point (14).

In this process, the appropriate stoichiometric ratios of strontium carbonate ($SrCO_3$, Merck), boric acid (H_3BO_3, Merck, 99.5%), samarium(III) oxide (Sm_2O_3, Sigma-Aldrich, 99.9%) and europium(III) oxide (Eu_2O_3, Sigma-Aldrich, 99.99%) were weighed, mixed and ground together, with a glass mortar and pestle. The mixture was placed in a crucible and annealed in an ambient atmosphere in a Chengyi CHY-1700 horizontal tube furnace at 700 °C for 5 h. A rate of 5 °C/minute was used for heating and cooling.

Once at room temperature the mixture was again ground and reduced at 850 °C in the furnace to obtain the final products. For the post-synthesis thermal annealing, a reducing atmosphere of 5% hydrogen – 95% argon with a 200 mL/minute flow rate was introduced. The reducing atmosphere facilitated the reduction of the dopant ions to the divalent state and in return enhanced the emission intensity of the Sm^{2+} ions as shown in Figure S1-2 in the supporting information (15). The reducing atmosphere also ensures purging of the atmosphere which prevents oxidation of the mixture (26).

Experimental Parameters

In a first set of experiments, the reduction time at 850 °C was varied from 0 h (no annealing), 3 h, 5 h, 10 h, to 20 h while keeping the molar ratio of boron (B, in the form of boric acid) to strontium (Sr) at 6:1. The molar ratios for both Eu and Sm ions to Sr were fixed at 0.05:1 (5). In a second set of experiments, B and Sr were added in different molar ratios. This B:Sr ratio was varied from 3:1, 4:1, 5:1, 6:1, 7:1, 8:1, to 9:1 while still fixing molar ratios for both Eu and Sm ions to Sr at 0.05:1. In the next experiment, the molar ratio of Sm:Sr was varied from 0.00:1, 0.01:1, 0.025:1, 0.05:1 to 0.1:1. The ratio of Eu:Sr was fixed at 0.05:1. Lastly, the molar ratio of Eu:Sr was varied from 0.00:1 0.01:1, 0.025:1, 0.05:1 to 0.01:1 while keeping the molar ratio Sm:Sr fixed. With every optimisation step the molar ratios and reduction time that yielded the best photoluminescence intensity performance were used as the standard for the subsequent experiments.

Characterisation

The structures of the samples were analysed by using X-ray diffraction (XRD) measurements. This was done using a Bruker D8 Advance AXS GmbH XRD with a Cu Kα source with average (between $K\alpha_1$ and $K\alpha_2$) wavelength λ of 1.5406 Å and an instrumental broadening profile β_i of 0.033° (@ 28°). The Scherrer equation, given in Equation 7, was used to determine the crystallite size L of the samples reduced for different periods. In this equation K depends on the crystallite shape and is typically taken to be 0.9 and θ_β is the Bragg angle of a specific peak in the XRD profile (27). The full width at half maximum (FWHM) for a specific peak β is determined by using Equation 8 where β_m is the measured FWHM of a particular peak. The powder diffraction file (PDF) numbers of the XRD standards considered are as follows: SrB_2O_4: 00-015- 0779, SrB_4O_7: 00-015-0801, SrB_6O_{10}: 00-020-1190.

$$L = \frac{K\lambda}{\beta \cos\theta_\beta}$$

Equation 7

$$\beta^2 = {\beta_m}^2 - {\beta_i}^2$$

Equation 8

A JEOL JSM-7800F field emission scanning electron microscope (FE-SEM) with a primary beam voltage of 5 kV and a working distance of 10.0 mm was used to image the particle morphology. Samples were coated with iridium to avoid charging.

The steady-state excitation and emission, luminescence decay and quantum efficiency measurements were performed at room temperature using an Edinburgh Instruments FS5 Spectrofluorometer and an FLS980 Photoluminescence Spectrometer. These instruments use xenon lamps as the excitation source for steady-state measurements. They also use correction factors to correct for changes in the intensity of the excitation source and spectral sensitivity of the emission detector. The FLS980 system is also equipped with an integrating sphere which also utilises correction factors to include the optical response of the surface of the sphere. While studying the steady-state emission of the Eu^{2+} and Sm^{2+} ions, a standard excitation wavelength of 325 nm was used, while for the Eu^{3+} and Sm^{3+} ions an excitation wavelength of 240 nm was used.

The FLS980 system was used with a 255 nm picosecond 50 kHz light emitting diode (LED) excitation source for the luminescence decay measurements. The decay time of the LED is 0.8 ns while the detector has a response time of 0.6 ns. The luminescence decay of ions can occur through multiple independent processes N, which results in a complex decay curve. Equation 9 was used to fit and model the experimental decay profiles. Here $I(t)$ represents the sum of luminescence intensities at a specific time t after the termination of the excitation source. $I_0(\tau_i)$ is the luminescence intensity $t = 0$ for

component i while τ_i is the corresponding emission decay constant. The luminescence decay profiles of the different compounds were analysed using the Fluorescence Analysis Software Technology (FAST) analysis program, which can fit multi-exponential functions to determine the values of both $I_0(\tau_i)$ and τ_i. The intensity-weighted average emission decay constant $\langle\tau\rangle$ is determined using Equation 10 (29).

$$I(t) = \sum_{i=1}^{N} \left[I_0(\tau_i) \exp\left(\frac{-t}{\tau_i}\right) \right]$$

Equation 9

$$\langle\tau\rangle = \frac{\sum I_0(\tau_i)\tau_i{}^2}{\sum I_0(\tau_i)\,\tau_i}$$

Equation 10

A Perkin Elmer Lambda 950 UV-VIS spectrometer was used to measure the diffuse reflectance spectra of the samples. This system uses Spectralon as standard reference sample. An in-house modified 325 nm He-Cd laser photoluminescence system was used for the low temperature measurements (28). This system uses an Advanced Research Systems (ARS) closed-cycle cryostat system with a heater element for low temperature-dependent photoluminescence measurements.

To obtain information on the oxidation states of the Eu and Sm ions, X-ray spectroscopy was performed at the ID26 beamline at the European Synchrotron Radiation Facility (ESRF) (30). High Energy Resolution Fluorescence Detected X-ray Absorption Near Edge Structure (HERFD-XANES) spectra were obtained at the Eu L_3 (6.9769 keV) and Sm L_3 (6.7162 keV) absorption edges (31). The incident energy was selected with a silicon (311) double crystal monochromator. An X-ray emission spectrometer based on Rowland geometry was used with five spherically bent germanium (333) crystal analysers, aligned to the Eu $L\alpha_1$ (5.846 keV) and Sm $L\alpha_1$ (5.636 keV) energies (32). The samples were prepared by diluting them in cellulose with a 1:1 mass ratio and then pressing them into a pellet form. It was verified that the spectra were not influenced by x-ray induced changes. All this was done to ensure that the obtained oxidation states are representative of the as-prepared powders. HERFD-XANES spectra at the Eu L_3 and Sm L_3 absorption edges feature a recurrent energy difference of about 7 - 8 eV between the white lines that correspond to divalent and trivalent ions (33). This enabled a straightforward assessment of the relative divalent and trivalent ion concentration that scales with the respective intensity ratio.

Results and Discussion

Reduction time

The first parameter that was investigated was the reduction time at 850 °C while keeping the molar ratio of B:Sr at 6:1 and the Eu and Sm ions fixed at 0.05:1. This parameter was varied from 0 h, 3 h, 5 h, 10 h, to 20 h. Figure 2 compares the XRD reflection patterns of the different samples with the standards. All the compounds consist of a mixture of SrB_4O_7 and SrB_6O_{10} phases. SrB_4O_7 was present due to the evaporation of some of the boron oxide (B_2O_3) during synthesis, which other studies (5), (34), (35) also have noted. B_2O_3 is one of the reaction products of H_3BO_3 when this is heated to elevated temperatures (36). Due to the evaporation of some of the B_2O_3, the molar ratio of B with respect to Sr used before synthesis was not necessarily reflected in the obtained stoichiometry of the products.

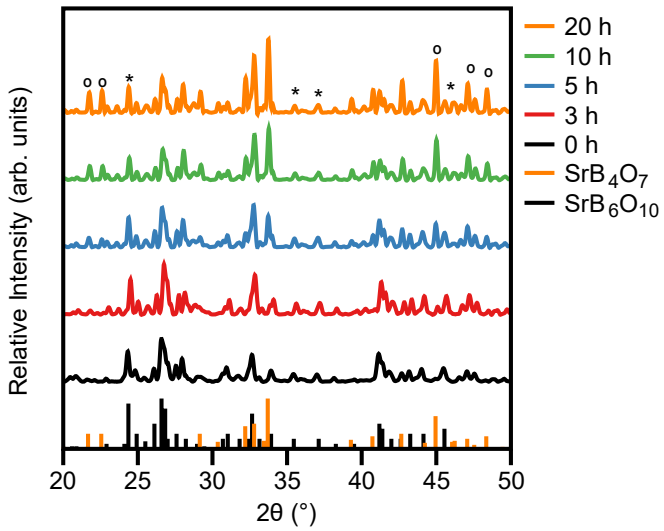

*Figure 2: X-ray diffraction reflection patterns of strontium borate materials prepared with a molar ratio of B: Sr at 6:1 and reduced for different periods. Given at the bottom are the x-ray diffraction standards. The crystallite sizes for strontium tetraborate and strontium hexaborate structures were measured using the reflections marked with º and *, respectively.*

As seen in Figure 2, longer reduction times promoted the formation of the SrB_4O_7 structure. The fraction of SrB_4O_7 and SrB_6O_{10} was estimated as 8% and 92% for the 0 h sample while for the 20 h sample the fraction was estimated as being 46% and 54%, respectively. These estimates were calculated by comparing the intensities of specific reflections with those of prepared standards for each structure.

Using Equation 7 and Equation 8 the crystallite size of the different samples for both the SrB_4O_7 and SrB_6O_{10} structures were calculated as explained in the Experimental and Methodology section. This was done by measuring the FWHM of the reflections marked with º and * in Figure 2. These reflections were selected since they do not overlap with other nearby diffraction peaks and therefore should provide a good representation of both structures present in the samples.

Figure 3 shows the average crystallite size as a function of the reduction time for both structures. The crystallite size of the SrB_4O_7 structure was on average 20 - 30% larger than that of the SrB_6O_{10} structure. The SrB_4O_7 structure shows a 37% growth while the SrB_6O_{10} structure shows a 24% growth in crystallite size when comparing the 20 h sample to the unreduced sample. The crystallite growth rate of both structures seems to slow down above a reduction time of 5 hours.

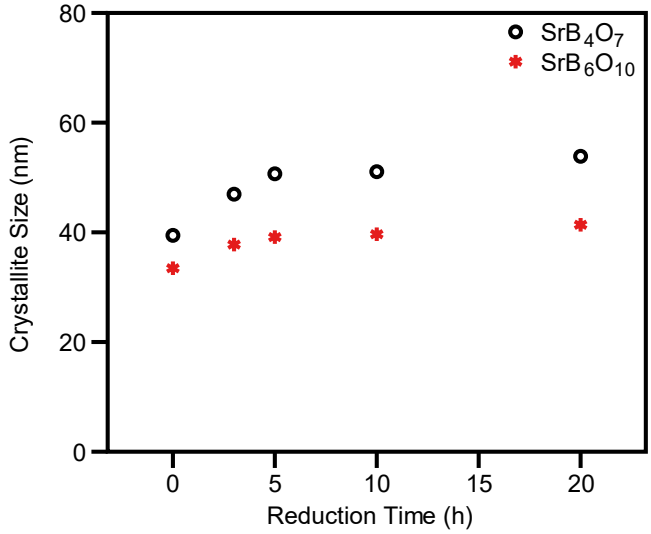

Figure 3: Crystallite sizes of the strontium tetraborate and strontium hexaborate compounds reduced for different periods. These values were calculated by using the Scherrer equation.

Figure 4 a) shows the emission spectra of the samples. The deep red emission from the Sm^{2+} ions dominated all the spectra, which correlates with the intraconfigurational-$4f^6$ transitions shown in the partial energy diagram for Sm^{2+} ions in Figure 1 a). The spectral position of the Sm^{2+} ion's emission spectra did not significantly change, including no additional splitting of the $^5D_0 - {}^7F_J$ transitions and no relative intensity changes was observed. The unchanged spectral position makes sense since the intra-configurational $4f^6$ emissions are only weakly sensitive to the chemical environment due to the filled 5s and 5p shells that shield the 4f electrons. Therefore, changes in the composition did not affect the spectral position of the Sm^{2+} related emission.

There was, however, a substantial variation in the emission intensity of the Sm^{2+} ions, as shown in Figure 4 a). The emission intensity increased and levelled off as a function of the reduction time. The corresponding XRD analysis showed the increase in crystallite size that can explain the Sm^{2+} ions emission intensity enhancement. Emission from the Eu^{3+} ions was observed for the 0 h sample as shown in Figure S2-3 in the supporting information. This emission was not present with all the samples reduced at 850 °C, which could be due to intervalence charge transfer quenching due to the presence of Eu^{2+} (37). The supposed reduction of the ions to the divalent state can also contribute to the enhancement of the Sm^{2+} ions emission intensity.

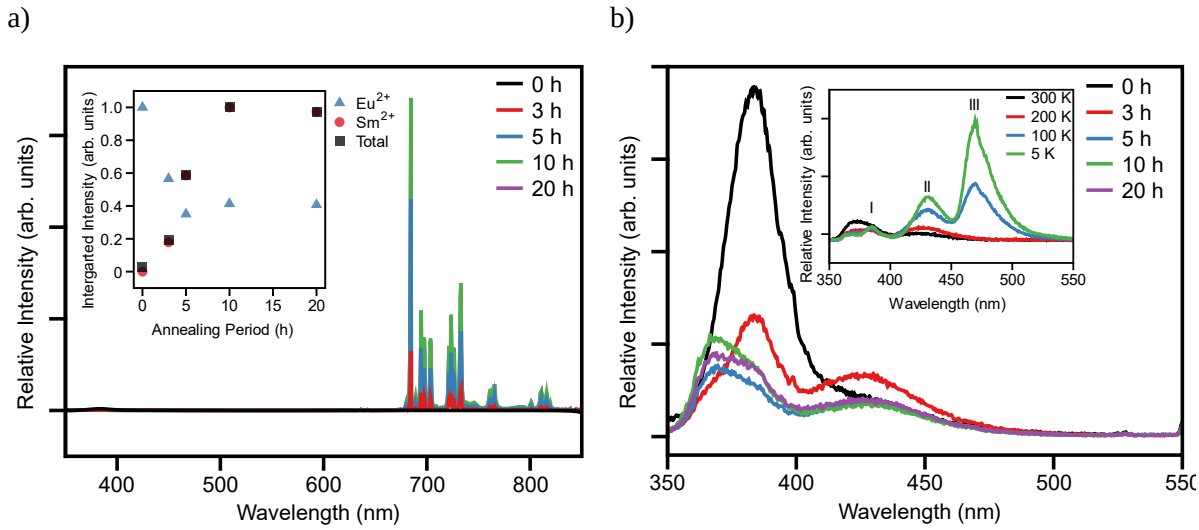

Figure 4: a) Emission spectra excited at 325 nm of strontium borate doped with europium and samarium ions, reduced for different periods. Both europium and samarium have a molar ratio of 0.05:1 to strontium. Inset shows the integrated emission intensity from the divalent europium (350 nm to 550 nm) and samarium (650 nm to 850 nm) ions and the total integrated emission intensity for the entire emission spectrum. These intensities for Eu^{2+}, Sm^{2+} and the total emission are shown as a fraction of the integrated intensity of the sample that emits the highest intensity for Eu^{2+}, Sm^{2+} and total emission, respectively. b) Room temperature emission spectra of divalent europium ions. Inset shows the measured emission spectra of the sample reduced for 5h, cooled to different temperatures and excited with 325 nm laser radiation. The labels show the emission of the divalent europium ions associated with different sites within strontium hexaborate.

In the region between 350 to 550 nm in Figure 4 a), some relatively weak emissions from Eu^{2+} ions are visible, mainly between 350 and 480 nm. Figure 4 b) shows the emission from the Eu^{2+} ions in more detail. It shows that the spectra consist of several peaks that can be deconvoluted into multiple components. As seen in the inset in Figure 4 b), when cooled to cryogenic temperatures, three distinct peaks became visible in the emission spectrum of the Eu^{2+} ions. These three peaks correlate with the Eu^{2+} ions in three different crystallographic sites in the SrB_6O_{10} host (26). Each site has a specific ligand field which has a distinct influence on the $4f^65d^1$ - $4f^7$ band that results in a variation in the position of the emission peak, as explained in the Theory and Literature Review section. The respective decrease and absence of peaks II and III in the intermediate and room temperature spectra suggests that the lower energy emission bands have a stronger thermal quenching behaviour. In the inset of Figure 4 b) the peak labelled I at 5 K has a high energy shoulder that peaks at 368 nm. This shoulder is due to Eu^{2+} ions in the SrB_4O_7 structure. This structure has only a single crystallographic site in which the Eu^{2+} ions are situated (24). This promotion of the SrB_4O_7 structure, as shown in the XRD analysis, corresponds with the Eu^{2+} peak shifting towards the high energy, as seen in Figure 4 b).

For the remaining optimisation process, a standard reduction time of 10 h was used. This reduction time proved to sufficiently aid in crystallite growth which resulted in enhanced emission from the Sm^{2+} ions.

For this reduction time, the fractions of SrB_6O_{10} and SrB_4O_7 were estimated as 61% and 39%, respectively. To improve the phase purity of the compounds, it is essential to control the formation of the different structures. The molar ratio of B:Sr was varied to achieve this.

Boron Concentration

The following parameter that was investigated was the molar ratio of B with respect to Sr. This parameter was varied from 3:1, 4:1, 5:1, 6:1, 7:1, 8:1, to 9:1 while keeping the Eu and Sm to Sr ratios fixed at 0.05:1 and using a reduction time at 850 °C of 10 h. Figure 5 compares the XRD reflection patterns of a selection of the different compounds that were prepared with the XRD standards. The structure of the material changed as a function of the molar ratio of B with respect to Sr. When compared to the standards, it was observed that at a ratio of 3:1 the compounds primarily consisted of SrB_2O_4 together with some SrB_4O_7. Increasing the amount of B:Sr to a ratio of 5:1 changed the compound to a dominant SrB_4O_7 phase with some SrB_2O_4 and SrB_6O_{10}. Primarily the SrB_6O_{10} phase was obtained when the ratio was increased to more than 7:1.

As shown in Figure 5 increasing the ratio to 9:1 did not yield any new phases like SrB_8O_{13}. However, a broadening in the XRD peaks can be observed, which indicates a decrease in the material's crystallite size. Figure 6 shows the FE-SEM images of the same selection of materials. These images illustrate how the materials prepared with low B:Sr ratios have well-defined morphologies. However, those prepared with high ratios have a pebble-like structure that is enclosed by a featureless morphology.

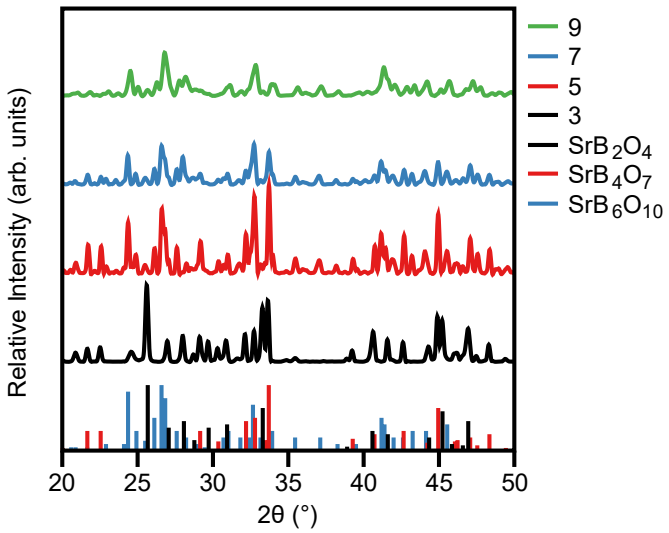

Figure 5: X-ray diffraction reflection patterns of a selection of strontium borate synthesised with different molar ratios of boron with respect to strontium. Given at the bottom are the x-ray diffraction standards for a selection of strontium borate structures.

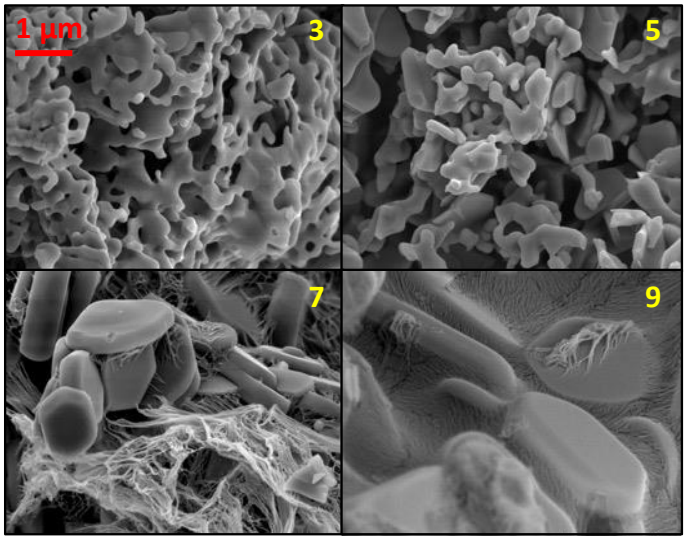

Figure 6: FE-SEM images of a selection of strontium borate compounds synthesised with different molar ratios of boron with respect to strontium (molar ratios are indicated on the top right in the images). The scale is the same for all the images.

Figure 7 a) shows the emission spectra from the Eu^{2+} and Sm^{2+} ions, while the inset shows the corresponding integrated intensity from the two ions and the total emission as a function of the B to Sr ratio. The emission intensity from the Sm^{2+} ions increased and reached a maximum at a molar ratio of 7:1. The increase in emission intensity can be attributed to the change in phase of the compounds, as shown by the XRD analysis. No additional splitting of the $^5D_0 - {}^7F_J$ transitions of the Sm^{2+} ions was observed as shown in zoomed in emission spectra in Figure S2-4 in the supporting information.

Figure 8 shows the emission spectra of the Sm^{3+} ions, obtained by exciting the compounds at 240 nm, where Sm^{2+} excitation was at its weakest, as seen in Figure 1 b). The emission spectra consist of the $^4G_{5/2} - {}^6H_J$ transitions of the Sm^{3+} ions (35). The intensity of these emission peaks decreased with an increase in the B to Sr ratio. This is because the ability of the SrB_4O_7 and SrB_6O_{10} structures to stabilise the divalent Sm ions is higher than that of the SrB_2O_4 structure. This decrease in the emission intensity from the Sm^{3+} ions can explain the resulting increase in the emission intensity from the Sm^{2+} ions.

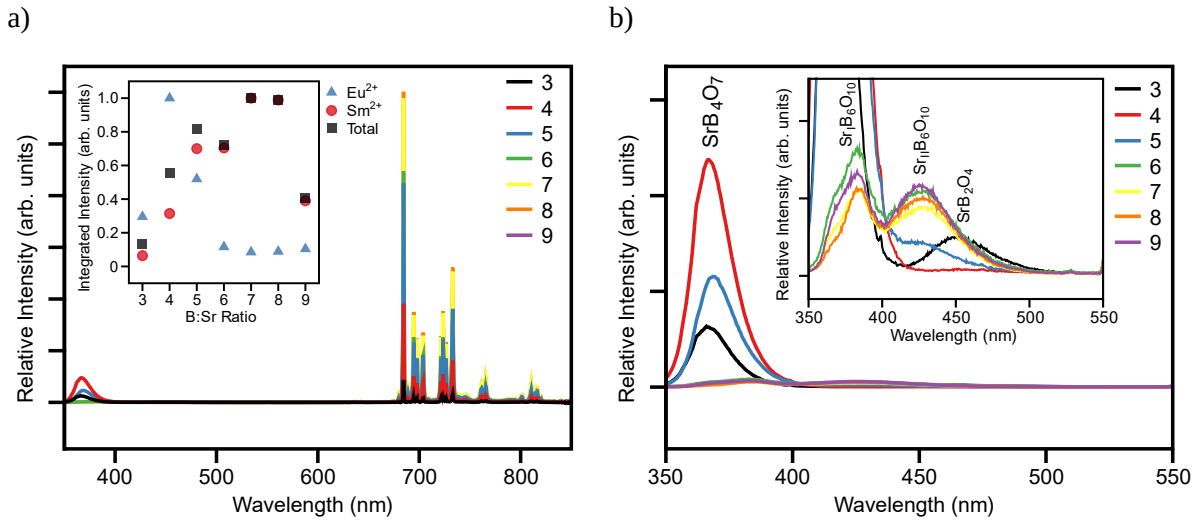

Figure 7: a) Emission spectra excited at 325 nm of strontium borate compounds doped with europium and samarium synthesised with different molar ratios of boron. Both europium and samarium have a molar ratio of 0.05:1 to strontium. The numbers in the legend refer to the B:Sr molar ratio. Inset shows the integrated emission intensity from the divalent europium (350 nm to 550 nm) and samarium (650 nm to 850 nm) ions and the total integrated emission intensity for the entire emission spectrum. These intensities for Eu^{2+}, Sm^{2+} and the total emission are shown as a fraction of the integrated intensity of the sample that emits the highest intensity for Eu^{2+}, Sm^{2+} and total emission, respectively. b) Emission spectra of divalent europium ions. The numbers in the legend refer to the B:Sr molar ratio. Inset shows a detailed view of the of the same region. The labels show the emission of the divalent europium ions associated with different host structures and different sites.

Figure 7 b) shows this emission from Eu^{2+} ions in the region between 350 to 550 nm in more detail. A substantial decrease in the intensity of the Eu^{2+} emission occurred. This decrease can imply an increase in the energy transfer to the Sm^{2+} ions (15). Figure 7 b) also shows a change in wavelengths for the Eu^{2+} emission peak, which indicates a change in the ion's ligand field. This change results from a variation in the structure of the host material, as suggested by the XRD analysis. The peaks associated with Eu^{2+} ions in the different host structures and sites are also indicated (38).

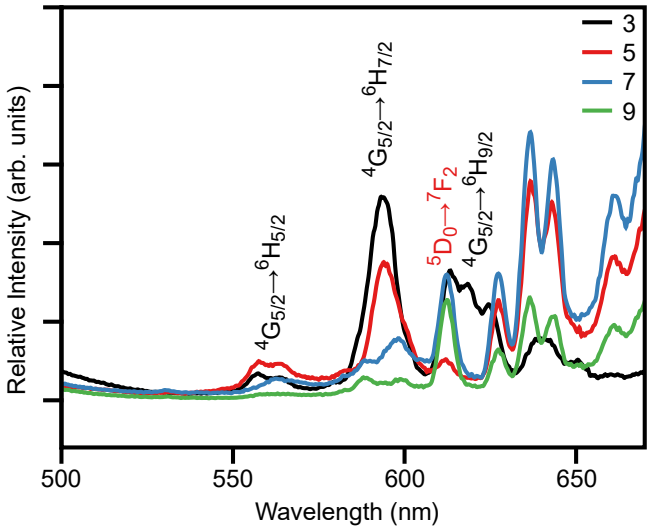

Figure 8: Emission spectra excited at 240 nm of a selection of strontium borate compounds synthesised with different molar ratios of boron. The numbers in the legend refer to the B:Sr molar ratio. Both europium and samarium have a molar ratio of 0.05:1 to strontium. Black and red labels indicate transitions associated with trivalent samarium and trivalent europium ions, respectively, while unlabelled peaks are related to transitions from the higher $^5D_1$ level of the divalent samarium ions.

One of the limitations of luminescence spectroscopy is that it can only give qualitative information on the amount of dopant ions in each oxidation state (24). This is due to effects such as energy transfer and non-ideal quantum efficiencies that can affect the photoluminescence intensity of specific ions. Therefore X-ray spectroscopy (HERFD-XANES) was used to obtain quantitative information on the oxidation state of the Sm and Eu ions for the different samples as explained in the Experimental and Methodology section. As seen in Figure 9 a), there was a substantial increase in the fraction of Eu^{2+} ions with an increase in the molar ratio of boron, which reached a maximum at a molar ratio of 7:1. This again confirms the fact that SrB_4O_7 and SrB_6O_{10} have a higher ability to stabilise the divalent ions when compared to SrB_2O_4.

A similar trend, peaking at a molar ratio of 7:1, occurred with the Sm ions in Figure 9 b). However, a relatively low fraction of Sm^{2+} ions was present in all the samples when compared to the fraction of Eu^{2+} ions. This is due to the reduction potential of Sm ($E^*_{Sm^{3+}/Sm^{2+}}$ = -2.17 V) being lower than the reduction potential of Eu ($E^*_{Eu^{3+}/Eu^{2+}}$ = -0.76 V) (39). In both figures a change in the shape of the high energy side is seen, which can be linked to the changes in the composition of the material.

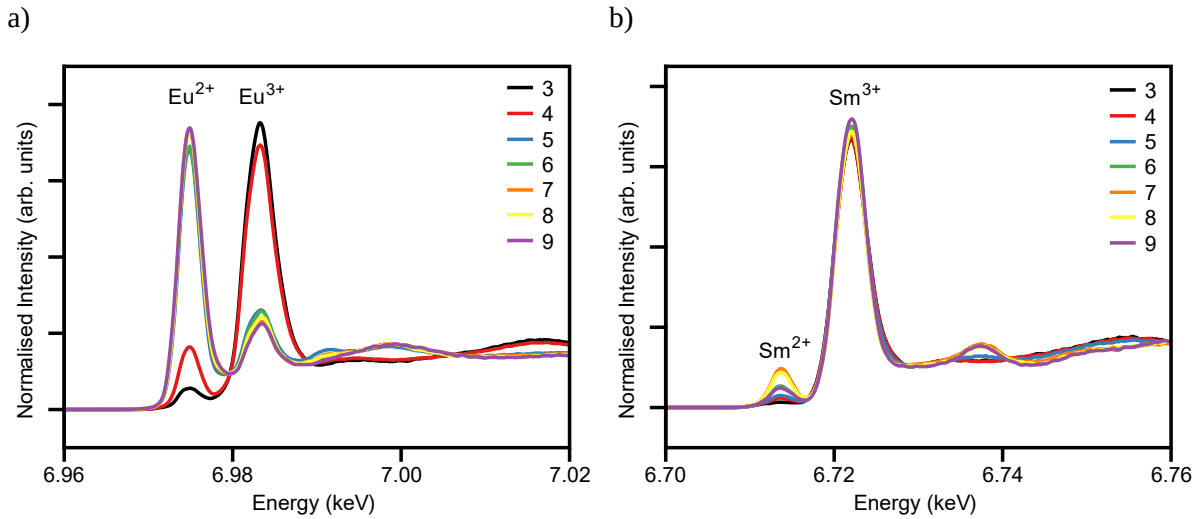

Figure 9: a) Europium and b) samarium L_3 absorption edge HERFD-XANES spectra for divalent and trivalent ions of strontium borate compounds synthesised with different molar ratios of boron. The numbers in the legend refer to the B:Sr molar ratio.

When comparing the emission spectra in Figure 7 and the XRD reflection patterns in Figure 5 it can be concluded that the Sm^{2+} ions in the SrB_6O_{10} phase yield a higher emission intensity than those in the SrB_4O_7 phase. This same experimental result was also observed in a study by Runowski et al. (10). However, in that study the authors postulated that the stabilisation of the Sm ions in the divalent state is preferred in the more complex borate matrix. This explanation is questionable, since as explained in the Theory and Literature Review section and proven by the HERFD-XANES results, both these structures have similar ability to stabilise divalent dopant ions.

The excitation spectra of the Sm^{2+} ions are shown in Figure 10. The region between 230 nm and 360 nm mimics the same form seen in the excitation spectrum of Eu^{2+} ions shown in Figure 1 b). Therefore, this region indicates that excitation of the Eu^{2+} ions can be followed by energy transfer to the Sm^{2+} ions. The region from 300 nm to 600 nm consists of the $4f^6$ - $4f^55d^1$ band of the Sm^{2+} ions (14). Figure 10 shows the relative enhancement of the direct excitation of Sm^{2+} ions at higher ratios of B:Sr. A possible reason for this is that the ligand field of the SrB_6O_{10} structure enhances the $4f^6 – 4f^55d^1$ excitation band of the Sm^{2+} ions. This was confirmed by measuring the diffuse reflectance spectra of the samples as explained in the Experimental and Methodology section. Figure 11 shows that the absorption increased as with an increase in the B:Sr ratio.

Due to a higher spectral overlap of the emission of Eu^{2+} ions and the excitation of Sm^{2+} in the SrB_6O_{10} host, a more substantial energy transfer can occur. This enhanced energy transfer and increased absorption resulted in a 220% increase in the emission intensity of the Sm^{2+} ions in the SrB_6O_{10} host compared to the SrB_4O_7 host (λ_{ex} = 325 nm). The amorphous phase formation at the highest B:Sr ratio

drastically reduced the optical performance of the compound and resulted in the decrease in the emission intensity of the Sm^{2+} ions.

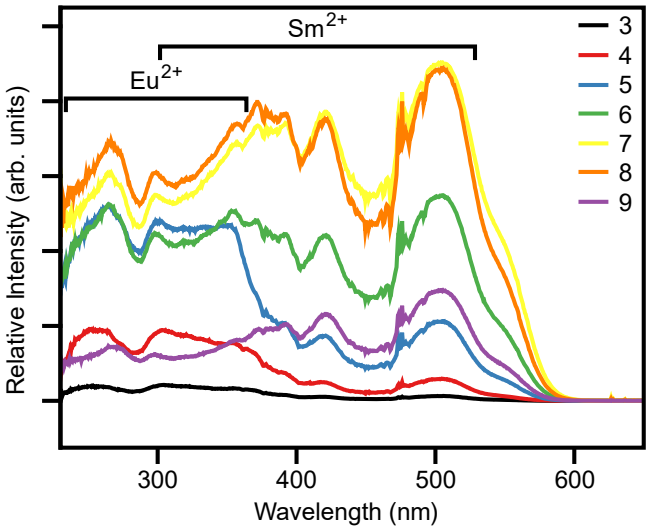

Figure 10: Excitation spectra of divalent samarium ions probed at 684.5 nm within strontium borate compounds synthesised with different molar ratios of boron. The brackets indicate the dominant excitation regions for the respective divalent ions. The numbers in the legend refer to the B:Sr molar ratio.

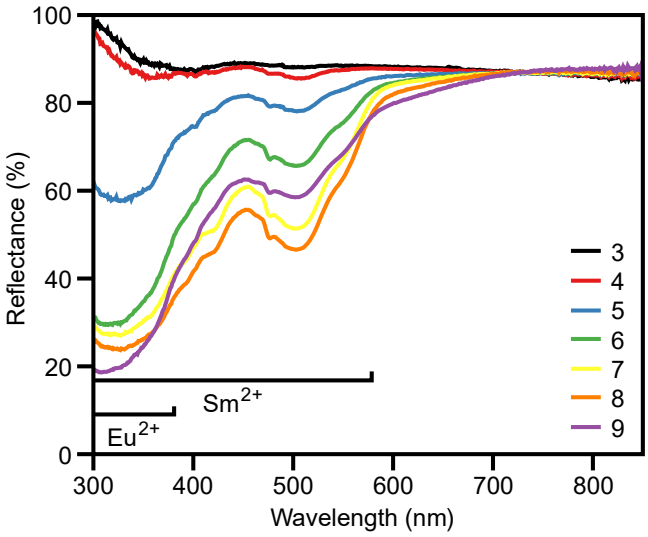

Figure 11: Diffuse reflectance spectra of strontium borate compounds doped with europium and samarium synthesised with different molar ratios of boron. The brackets indicate the dominant absorption regions for the respective divalent ions. The numbers in the legend refer to the B:Sr molar ratio.

A molar ratio of 7:1 was used for the remaining optimisation process since this yielded the purest phase of SrB_6O_{10} structure and resulted in the highest Sm^{2+} ion emission. This structure also gave rise to an excitation spectrum that peaks at longer wavelengths that can more effectively utilise the broad solar spectrum (1). Unfortunately, little information on this structure is available and it has also not yet been fully elucidated (34). The following section examines the energy transfer process in more detail by varying the concentrations of the Sm and Eu ions.

Samarium Concentration

To better understand the energy transfer between the divalent ions, and to determine the critical energy transfer distance and critical distance between the Sm ions, the molar ratio of the Sm ions with respect to Sr were varied from 0:1, 0.01:1, 0.025:1, 0.05:1 to 0.1:1 while keeping the Eu concentration with respect to Sr fixed at 0.05:1. As seen in the XRD reflection patterns of the different compounds in Figure S3-5 in the supporting information, there is leftwards shift in the patterns with an increase in the moral ratio of Sm. This is due to the increase in the lattice parameters which is caused by the presence of the Sm ions. As stated in the Theory and Literature Review section Sm^{2+} ions have a larger ionic radius than the Sr^{2+} ions it replaces.

Figure 12 shows the emission spectra of these compounds. When no Sm ions were present only the emission from Eu^{2+} ions was observed. Even when a tiny amount of Sm ions was added, the emission from Sm^{2+} ions became noticeable. In contrast, upon the introduction of Sm ions, the emission from the Eu^{2+} ions was drastically reduced, which indicates energy transfer from the Eu^{2+} ions to the Sm^{2+} ions.

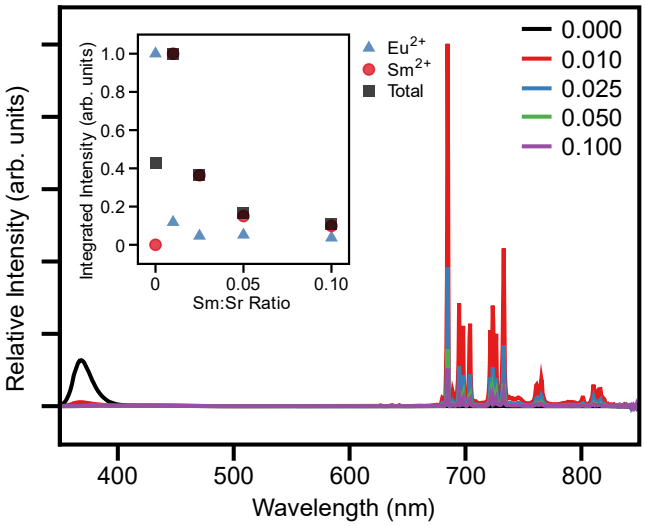

Figure 12: Emission spectra excited at 325 nm of strontium borate synthesised with different molar ratios of samarium to strontium (indicated in the legend). The europium molar ratio was kept constant at a ratio of 0.05:1 with respect to strontium. Inset shows the integrated emission intensity from the divalent europium (350 nm to 550 nm) and samarium (650 nm to 850 nm) ions and the total integrated emission intensity for the entire emission spectrum. These intensities for Eu^{2+}, Sm^{2+} and the total emission are shown as a fraction of the integrated intensity of the sample that emits the highest intensity for Eu^{2+}, Sm^{2+} and total emission, respectively.

The luminescence decay profiles of the emission from the Eu^{2+} ions were measured as described in the Experimental and Methodology section. Figure 13 compares the luminescence decay profile of the solely Eu-doped compound with the 0.01:1 compound. There is a significant difference between the two profiles and both show a non-exponential character. This non-exponential nature can be due to the

strongly overlapping emission bands of the Eu^{2+} ions in the different sites of the SrB_6O_{10} host material (40).

The decay profiles were analysed, and it was determined that the solely Eu-doped compound had an average decay time of 2.20 µs. By using Equation 1 together with Equation 2, and estimating the refractive index of the SrB_6O_{10} host material as 1.61, the decay time for the Eu^{2+} ions could be estimated as being in the order of 0.5 µs. The value for estimated refractive index is based on the refractive indexes of SrB_2O_4 (41), SrB_4O_7 (42) and SrB_8O_{13} (40) host materials. The reason for this significant increase in the measured decay time compared to the estimated one, can be due to the relatively high concentration of Eu ions which leads to energy transfer between the sensitiser ions. According to a study by Poort et al. energy transfer between Eu^{2+} ions can result in an increase in the decay time (19). The measured decay times agree with the values of 2.388 µs to 1.649 µs determined in a similar experiment for the SrB_4O_7 structure by Zheng et al. (43). In that study a europium molar ratio of 0.05:1 with respect to strontium was also used.

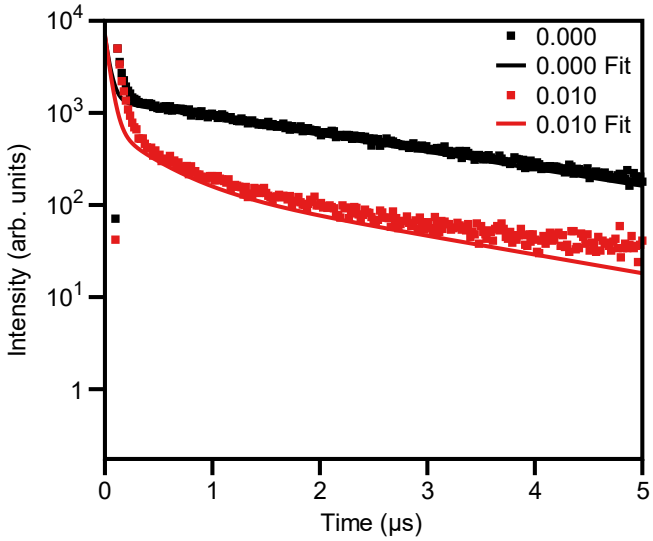

Figure 13: Luminescence decay profiles at room temperature, measured at 385 nm for strontium borate synthesised with different molar ratios of samarium to strontium (indicated in the legend). The europium molar ratio was kept constant at a ratio of 0.05:1 with respect to strontium. The excitation source is a 255 nm pulsed LED. The solid lines indicate the fitting that was done to the data sets.

The luminescence decay profiles were measured as a function of the molar ratio of the Sm ions. The results of the lifetime profiles are tabulated in Table 2. The average decay time decreased as a function of the molar ratio of the Sm ions, which verifies that energy transfer occurs from the Eu^{2+} to Sm^{2+} ions. Using Equation 3 the energy transfer efficiency was calculated and tabulated in Table 2. A single exponential decay profile was measured for the Sm^{2+} ion's emission at 684.5 nm, also with 255 nm excitation, with a decay time of 3.7 ms. This value was measured for all the samples. This is in accordance with the value of 3.9 ms measured by Sun et al. for Sm^{2+} in the SrB_4O_7 structure (14).

Table 2: Resulting initial luminescence intensities ($I_0(\tau)\tau$) and decay times (τ) determined using the FAST analysis program for each compound measured at 385 nm. This program uses Equation 9 to determine these terms mathematically. The initial luminescence intensities are given as a percentage of the total of all the components. The average decay time ($\langle\tau\rangle$) the energy transfer efficiency (η_{ET}) for each compound was calculated using Equation 10 and Equation 3 respectively.

Sm:Sr	τ_1 (µs)	$I_0(\tau_1)\tau_1$ (%)	τ_2 (µs)	$I_0(\tau_2)\tau_2$ (%)	τ_3 (µs)	$I_0(\tau_3)\tau_3$ (%)	$\langle\tau\rangle$ (µs)	η_{ET} (%)
0.000	0.04	6			2.35	94	2.20	-
0.010	0.05	33	0.40	20	2.15	47	1.11	50
0.025	0.03	44	0.14	15	2.58	41	1.09	50
0.050	0.03	41	0.08	19	2.44	40	0.99	55
0.100	0.03	42	0.12	15	2.80	43	1.24	44

Since energy transfer between the Eu^{2+} to Sm^{2+} ions was verified, the critical energy transfer volume can be determined. This was done by plotting the normalised emission intensity of Eu^{2+} ions as a function of Sm concentration, as shown in Figure 14. Using the values established from the linear regression, the critical volume can be determined using Equation 4. The critical energy transfer distance was determined as >1.2 (±0.9) Å by using the equation relating the volume of a sphere to its radius. This result is a less than the value of 8.6 Å determined by Kulshreshtha et al. for the same ions in the SrB_4O_7 structure (15). This result is a lower limit estimate since as seen in Figure 9 b) it can be assumed that there is still a substantial amount of Sm^{3+} ions present in the samples.

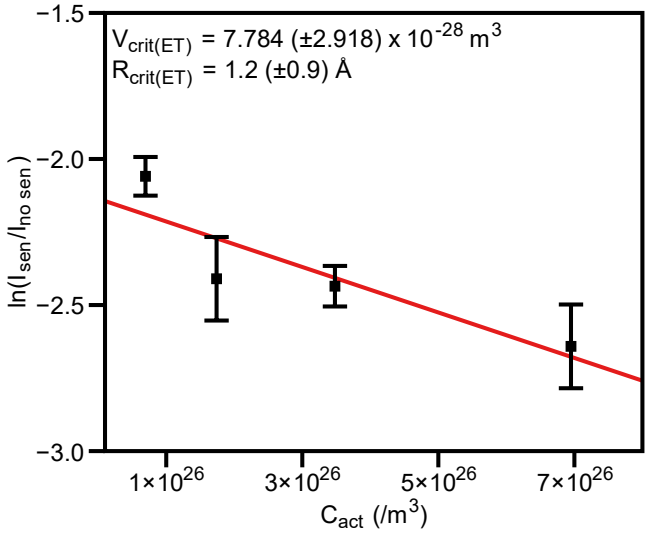

Figure 14: A linear regression fit of Reade's statistical model on the integrated emission intensity from the divalent europium (370 nm to 470 nm) as a function of the concentration of the samarium ions. The emission intensity was measured three times from which an average was determined. The error estimates indicate two standard deviations from the mean. The uncertainty of the fit was calculated using the standard error of the linear fit.

As seen in the inset of Figure 12, increasing the molar ratio of the Sm:Sr ions beyond 0.01 results in a strong decrease in the emission from the Sm^{2+} ions. This decrease in the emission intensity from the Sm^{2+} ions indicates a significant quenching process (21). This can result from concentration quenching of the luminescence, as explained in the Theory and Literature Review section. Intervalence charge transfer in Sm^{2+}/Sm^{3+} pairs is one possible underlying mechanism for the quenching process (44). This is supported by the fact that most Sm ions were incorporated in the trivalent state as shown by the HERFD-XANES result, and also by the relatively low concentration at which concentration quenching occurs (7).

In order to determine the critical distance between the Sm^{2+} activator ions the formal volume per possible crystallographic site for the activator ions was taken as 143.7 $Å^3$. The critical molar ratio for the activator ions was taken to be 0.01, which is the molar ratio of the Sm divalent and trivalent ions when the maximum emission intensity for the Sm^{2+} ion occurs of the samples that were synthesised. Using Figure 12 the critical distance between the Sm^{2+} activator ions was determined as >30.2 Å. This result agrees with the value of 29.8 Å determined by Tawalare et al. for Sm ions in the SrB_4O_7 structure (22). This result is also a lower limit estimate since as seen in Figure 9 b) it can be assumed that there is still a substantial amount of Sm^{3+} ions present in the samples. A molar ratio of 0.01:1 was used for the Sm ions for the remaining optimisation process since it yielded the highest Sm^{2+} ion emission as shown by the inset of Figure 12.

Europium Concentration

Lastly, the molar ratio of the Eu ions was varied from 0:1, 0.01:1, 0.025:1, 0.05:1 to 0.1:1 with respect to Sr while keeping the Sm concentration fixed at 0.01:1 with respect to Sr. As seen in the XRD reflection patterns of the different compounds in Figure S3-6 in the supporting information, there is rightwards shift in the patterns with an increase in the moral ratio of Eu. This is due to the decrease in the lattice parameters which is caused by the presence of the Eu ions. As stated in the Theory and Literature Review section Eu^{2+} ions has a smaller ionic radius than the Sr^{2+} ions it replaces.

Figure 15 shows the emission spectra at 325 nm excitation of the prepared phosphors. As shown in the inset, increasing the molar ratio of the Eu ions beyond 0.01 resulted in a decrease in the emission from the Eu^{2+} ions. Using Figure 15 the critical distance between the Eu^{2+} sensitiser ions was determined. This value is the same as for the Sm^{2+} activator ions. It is significantly higher than the value of 18.6 Å determined in the study by Zheng et al. (43). However, this result could be influenced by the energy transfer to the Sm^{2+} ions.

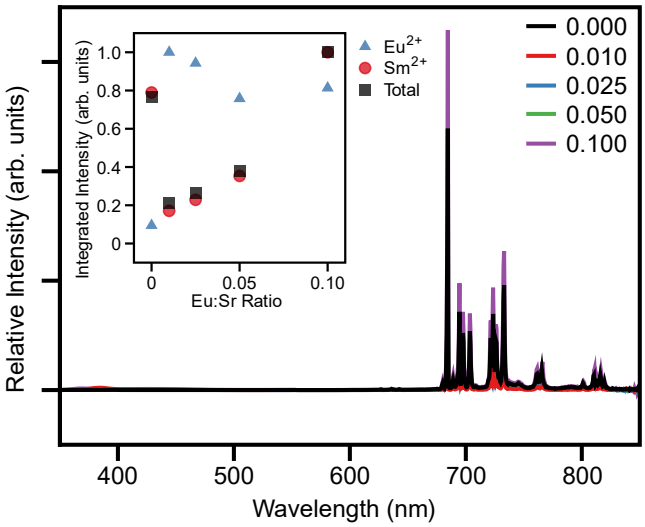

Figure 15: Emission spectra excited at 325 nm of strontium borate synthesised with different molar ratios of europium to strontium (indicated in the legend). The samarium to strontium molar ratio was kept constant at 0.01:1. Inset shows the integrated emission intensity from the divalent europium (350 nm to 550 nm) and samarium (650 nm to 850 nm) ions and the total integrated emission intensity for the entire emission spectrum. These intensities for Eu^{2+}, Sm^{2+} and the total emission are shown as a fraction of the integrated intensity of the sample that emits the highest intensity for Eu^{2+}, Sm^{2+} and total emission, respectively.

Figure 16 shows the excitation spectra of the Sm^{2+} emission. The same intensity trend at 325 nm occurs as seen for the Sm^{2+} ions in the inset in Figure 15. Only the broad excitation spectrum of Sm^{2+} is observed when no Eu ions are present. Upon introduction of the Eu ions, the region below 300 nm increased, which is expected; however, a significant decrease in the intensity was noticed where the excitation spectra of Eu^{2+} and Sm^{2+} overlap. This result can be due to Eu^{2+} ions which absorb excitation energy but do not successfully transfer it to the Sm^{2+} ions. However, with the further addition of Eu ions, the energy transfer process became more efficient which result in an increase in the intensity in the excitation spectrum of the Eu^{2+} ions.

As seen in Figure 16 the direct excitation of the Sm^{2+} ions increased with an increase in the molar ratio of Eu ions. Figure 17 shows the emission associated with Sm^{3+} and Eu^{3+} ions (labelled) and some emission associated with Sm^{2+} ions. The emission intensity of the Sm^{3+} ions drastically quenched upon the introduction of Eu. This result was also observed by Kulshreshtha et al., where Eu dopants were used to reduce and stabilise residual Sm^{3+} ions present in the material (15). This decrease in the amount of Sm^{3+} ions can possibly explain the increase in the direct excitation band of the Sm^{2+} ions.

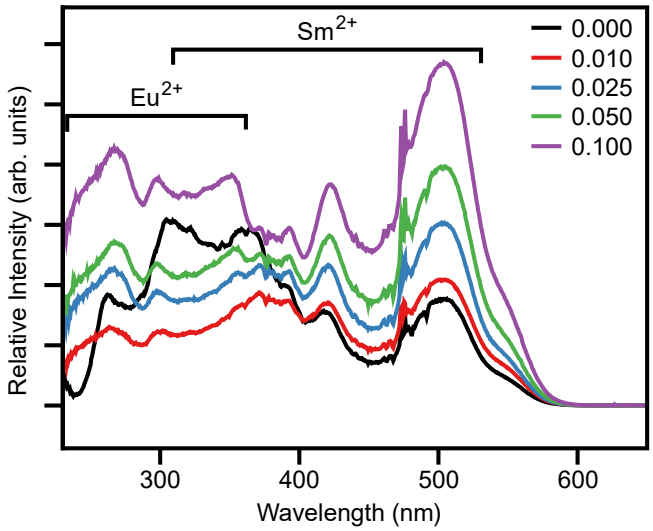

Figure 16: Excitation spectra of divalent samarium emission probed at 684.5 nm within strontium borate synthesised with different molar ratios of europium to strontium (indicated in the legend). The brackets indicate the dominant excitation regions for the respective divalent ions.

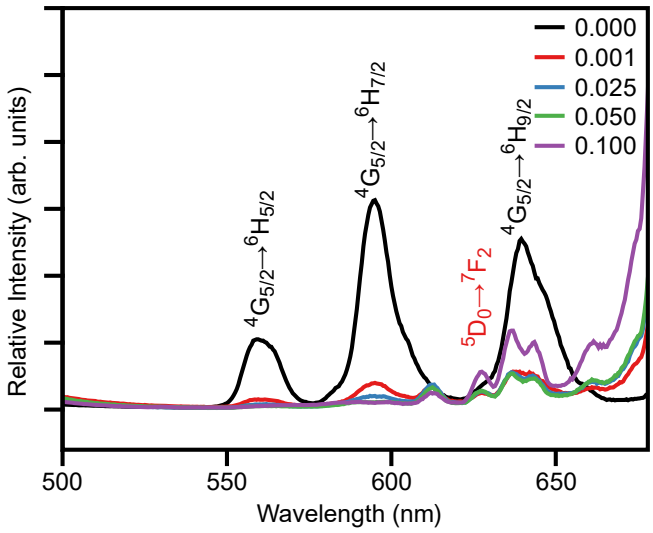

Figure 17: Emission spectra excited at 240 nm of strontium borate synthesised with different molar ratios of europium. The molar ratio of samarium was kept constant at 0.01:1 with respect to strontium. Black and red labels respectively indicate transitions associated with trivalent samarium and trivalent europium ions, while unlabelled peaks are related to transitions from the higher $^5D_1$ level of the divalent samarium ions.

This result agrees with the HERFD-XANES results (Figure 18), where a general increase in the fraction of Eu^{2+} and Sm^{2+} ions with an increase in the molar ratio of Eu ions was observed. This effect can possibly be explained by a charge compensation model as discussed in the Theory and Literature Review section and illustrated in Figure S1-1 in the supporting information. The increase in the molar ratio of the Eu ions causes an increase in the amount of vacancy defects at the Sr^{2+} sites. This leads to a larger availability of negative charges to reduce both the Eu and Sm ions to the divalent state.

This effect seems to be still dominant and increasing at relatively high Eu ion molar ratios. However, due to the scarcity and resultant high cost of the rare earth elements there is little practical use for highly doped phosphors in larger scale solar energy deployment (45). Therefore $Sr_{0.89}B_6O_{10}:Eu_{0.1}$, $Sm_{0.01}$ is considered as the optimised material in this study. In future studies this problem can possibly be addressed by incorporating other co-dopants in addition to Eu ions in order to enhance the Sm^{2+} emission. This strategy has yielded promising results as show in the study by Kulshreshtha et al. (15).

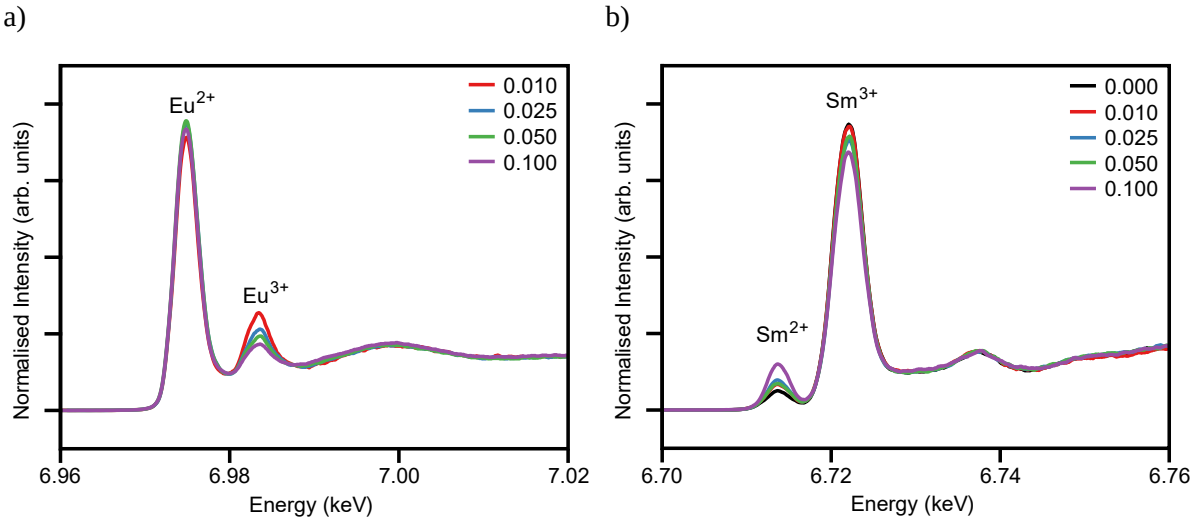

Figure 18: a) Europium and b) samarium L_3 absorption edge HERFD-XANES spectra for divalent and trivalent ions of strontium borate compounds synthesised with different molar ratios of europium

The internal luminescence quantum efficiency was determined of the optimised material by directly and indirectly exciting Sm^{2+} ions at 508.5 nm and 268.5 nm, respectively. The internal efficiency was determined as 79% and 17% for the direct and indirect excitation of Sm^{2+} ions, respectively. This significant difference between the direct and indirect excitation makes sense since the absorption and emission process within an isolated Sm^{2+} ion is much more efficient than energy transfer between Eu^{2+} ions and Sm^{2+} ions. This is also confirmed by the fact that the average energy transfer efficiency is 50% as calculated in Table 2. Energy migration between the high concentration of Eu^{2+} ions can also play a role as supported by the long luminescence lifetimes as given in Table 2. This energy transfer process between the Eu^{2+} ions can increases the probability for nonradiative energy losses (21).

Conclusions

Strontium borate phosphors co-doped with Eu and Sm ions were synthesised using a solid-state reaction method and characterised using XRD, steady-state excitation and emission, luminescence decay, low-temperature photoluminescence spectroscopy, diffuse reflectance spectroscopy, FE-SEM, and HERFD-XANES. The emission from the Sm^{2+} ions was optimised by varying the reduction time, the molar ratio of B, and the molar ratios of both lanthanide dopants. These experiments showed that a reduction time

of 10 h at 850 °C was sufficient to aid in crystallite growth which resulted in enhanced emission from the Sm^{2+} ions.

It was shown that different strontium borate host structures can be synthesised by varying the B:Sr molar ratio. From this it was shown that the SrB_6O_{10} structure can stabilise the Eu and Sm ions in the divalent state. The energy transfer between the divalent ions and the enhancement of the $4f^6 – 4f^55d^1$ excitation band of the Sm^{2+} ions was also higher when compared to the SrB_4O_7 structure. In a previous study by D. K. G. De Boer et al., the incorporation of Eu^{2+} and Sm^{2+} ions in the SrB_4O_7 structure was studied for solar conversion applications (5). However, considering the literature, the SrB_6O_{10} structure has not yet been studied in detail with this application in mind. This enhanced energy transfer and $4f^6 – 4f^55d^1$ excitation band resulted in a 220% increase in the emission intensity of the Sm^{2+} ions in the SrB_6O_{10} structure compared to the SrB_4O_7 structure (λ_{ex} = 325 nm).

To better understand the energy transfer between the divalent ions, the energy transfer efficiency, critical energy transfer distance and critical distance between the Sm ions were determined, by varying the molar ratio of the Sm ions. The resulting luminescence decay profiles of the Eu^{2+} ions were measured and a decrease from 2.20 µs to 1.11 µs for the average decay time was determined with the introduction of Sm ions. This verified the energy transfer between the ions. Using this result the average energy transfer efficiency was calculated as 50% while using Reade's statistical model, a lower limit for the critical energy transfer distance between the sensitiser and activator ions was determined as >1.2 (±0.9) Å. A lower limit for the critical distance between the Sm^{2+} activator ions was determined as >30.2 Å. Lastly, the molar ratio of the Eu ions was varied. This proved that higher Eu concentrations increased the energy transfer to the Sm^{2+} ions. Also, as observed by HERFD-XANES, the Eu ions aid in reducing the Sm ions to the divalent state by a charge compensation mechanism, which enhanced the direct excitation of the Sm^{2+} ions.

This study concludes that $Sr_{0.89}B_6O_{10}$:$Eu_{0.1}$, $Sm_{0.01}$ is the resulting optimised material. This material has a broad excitation region ranging from 220 nm to 600 nm and exhibited strong and narrow emission lines in the region from 650 nm to 850 nm. Also, the significant Stokes shift reduced the probability of reabsorption. An internal luminescence quantum efficiency of 79% (λ_{ex} = 508.5 nm) was measured. All these characteristics make this phosphor material a promising candidate for solar conversion and LSC applications.

Funding and Acknowledgements

This research work is supported by the South African Research Chairs Initiative of the Department of Science and Technology (84415). The financial assistance from the University of the Free State and Ghent University are also highly recognised. We acknowledge the European Synchrotron Radiation Facility (ESRF) for the allocation of beamtime (HC-4499 on beamline ID26, doi:10.15151/ESRF-ES-514011278). The financial support by the Fund for Scientific Research Flanders (FWO-Vlaanderen) via research grants G0H0417N and G0F9322N is appreciated.

References

1. Islam S. Analytical modeling of organic solar cells including monomolecular recombination and carrier generation calculated by optical transfer matrix method. Org Electron [Internet]. 2018;41(December 2016):143–56. Available from: http://dx.doi.org/10.1016/j.orgel.2016.10.040
2. M. Chegaar PM. Effect of atmospheric parameters on the silicon solar cells performance. J Electron Devices. 2018;6(January 2008):173–6.
3. Mazzucato S, Royall B, Ketlhwaafetse R, Balkan N, Salmi J, Puustinen J. Dilute nitride and GaAs n-i-p-i solar cells. Nanoscale Res Lett. 2012;7(631):1–5.
4. Day J, Senthilarasu S, Mallick TK. Improving spectral modification for applications in solar cells: A review. Renew Energy [Internet]. 2019;132:186–205. Available from: https://doi.org/10.1016/j.renene.2018.07.101
5. Boer DKG De, Broer DJ, Debije MG, Keur W, Meijerink A, Ronda CR, et al. Progress in phosphors and filters for luminescent solar concentrators. Opt Soc Am OCIS. 2011;021111:1197–9.
6. Yang C, Lunt RR. Limits of Visibly Transparent Luminescent Solar Concentrators. Adv Opt Mater. 2017;5(1600851):1–10.
7. Weber EMJ, Dotsenko A V, Glebov LB, Tsekhomsky VA. HANDBOOK OF OPTICAL Laser and Optical Science and Technology Series Physics and Chemistry of Photochromic Glasses. CRC Press; 2003.
8. Boer DKG De. Optimizing wavelength-selective filters for Luminescent Solar Concentrators Optimizing wavelength-selective filters for Luminescent Solar Concentrators. Photonics Sol Energy Syst III,. 2014;7725(May).
9. Shen YR, Bray KL, Holzapfel WB. Effect of temperature and pressure on radiative and nonradiative transitions of Sm^{2+} in SrFCl. J Lumin. 1997;72–74(96):266–7.
10. Przemysław W, Runowski M, Lis S. Influence of boric acid / Sr^{2+} ratio on the structure and luminescence properties (colour tuning) of nano-sized , complex strontium borates doped with Sm^{2+} and Sm^{3+} ions. Opt Mater J. 2018;83(February):245–51.

11. Wickleder C. Excited states of Sm^{2+} in chloride host lattices. J Lumin. 2001;95:127–32.
12. Zeng Q, Pei Z, Wang S, Su Q, Lu S. Luminescent Properties of Divalent Samarium-Doped Strontium Hexaborate. Am Chem Soc. 1999;11(14):605–11.
13. Weber EMJ, Kaminskii AA, Weber MJ, Weber MJ, Weber MJ. PHOSPHOR Physics and Chemistry of Photochromic Glasses. 2nd ed. CRC Press; 1998.
14. Jiayue SUN, Jicheng ZHU, Xiaotang LIU, Haiyan DU. Luminescence properties of $SrB_4O_7:Sm^{2+}$ for light conversion agent. J Rare Earths [Internet]. 2012;30(11):1084–7. Available from: http://dx.doi.org/10.1016/S1002-0721(12)60183-5
15. Kulshreshtha C, Cho SH, Jung YS, Sohn K. Deep Red Color Emission in an Sm^{2+}-Doped SrB_4O_7 Phosphor. J Electrochem Soc. 2007;154(3):86–90.
16. Stefani R, Maia ADS, Felinto MCFC, Brito HF. Highly enhanced luminescence of $SrB_4O_7:Eu^{2+}$ phosphor prepared by the combustion method using glycine as fuel. Opt Mater (Amst). 2007;29:1852–5.
17. Ma C, Brik MG, Liu D, Feng B, Tian Y, Suchocki A. Energy level schemes of f N electronic configurations for the di- , tri- , and tetravalent lanthanides and actinides in a free state. J Lumin J. 2016;170:369–74.
18. Joos JJ, Smet PF, Seijo L, Barandiarán Z. Insights into the complexity of the excited states of Eu-doped luminescent materials. Inorg Chem Front. 2020;7(4):871–88.
19. Poort SHM, Meyerink A, Blasse G. Lifetime measurements in Eu^{2+}-doped host lattices. J Phys Chem Solids. 1997;58(9):1451–6.
20. Kroon RE, Swart HC, Ntwaeaborwa OM, Seed Ahmed HAA. Ce decay curves in Ce, Tb co-doped LaF_3 and the energy transfer mechanism. Phys B Condens Matter. 2014;439:83–7.
21. Reade RF. Some Aspects of Sensitized Fluorescence in $Ca(PO_3)_2$:Sn:Mn Glass Phosphors. J Electrochem Soc. 1966;113(5):445.
22. Tawalare PK, Bhatkar VB, Omanwar SK, Moharil S V. $SrB_4O_7:Sm^{2+}$ phosphor for solar photovoltaics. AIP Conf Proc. 2019;2104(May 2021):3–8.
23. Suta M, Lavoie-Cardinal F, Wickleder C. Underestimated Color Centers: Defects as Useful Reducing Agents in Lanthanide-Activated Luminescent Materials. Angew Chemie - Int Ed. 2020;59(27):10949–54.
24. Pir P V, Dotsenko VP, Efryushina NP, Berezovskaya I V. Ln^{2+} Stabilization in Strontium Borates. Neorg Mater. 2006;42(8):994–1000.
25. Shannon RD. Revised Effective Ionic Radii and Systematic Study of Inter Atomic Distances in Halides and Chalcogenides in Halides and Chaleogenides. Acta Crystallogr. 1976;A 32:751–67.
26. Zeng Q, Pei Z, Wang S, Su Q. The reduction of Eu^{3+} in SrB_6O_{10} prepared in air and the luminescence of SrB_6O_{10}. J Alloys Compd. 1998;277:238–41.
27. Monshi A, Foroughi MR. Modified Scherrer Equation to Estimate More Accurately Nano-Crystallite Size Using XRD. World J Nano Sci Eng. 2014;(September 2012):154–60.

28. Erasmus LJB, Terblans JJ, Swart HC. Development of an optical thermometry system for phosphor materials. Vacuum [Internet]. 2018;(May):0–1. Available from: https://doi.org/10.1016/j.vacuum.2018.06.070
29. Li Y, Natakorn S, Chen Y, Safar M, Li DD. Investigations on Average Fluorescence Lifetimes for Visualizing Multi-Exponential Decays. Front Phys. 2020;8(October):1–13.
30. C. Gauthier, V. A. Sole, R. Signorato, J. Goulon EM. The ESRF Beamline ID26: X-ray Absorption on Ultra Dilute Sample. , J Synchrotron Radiat. 1999;6:164–6.
31. P. Glatzel, T. C. Weng, K. Kvashnina, J. Swarbrick, M. Sikora, E. Gallo, N. Smolentsev, R. Mori. Reflections on Hard X-Ray Photon-In/Photon-Out Spectroscopy for Electronic Structure Studies. J Electron Spectrosc. 2013;188:17–25.
32. Herbst JF, Wilkins JW. Relativistic calculations of 2p excitation energies in the rare-earth metals. Phys Rev B. 1982;26(4):1689–701.
33. Joos JJ, Van Der Heggen D, Amidani L, Seijo L, Barandiarán Z. Elucidation of the electron transfer mechanism in Eu^{2+} and Sm^{3+} codoped CaF_2: A step towards better understanding of trapping and detrapping in luminescent materials. Phys Rev B. 2021;104(20):31–5.
34. Liang H, Zeng Q, Hu T, Wang S, Su Q. Local structure and valences of samarium in SrB_4O_7:Sm and SrB_6O_{10}:Sm prepared in air. 2003;5:465–7.
35. Stefani R, Maia AD, Teotonio EES, Monteiro MAF, Felinto MCFC. Photoluminescent behavior of SrB_4O_7:RE^{2+} (RE ¼ Sm and Eu) prepared by Pechini , combustion and ceramic methods. J Solid State Chem. 2006;179:1086–92.
36. Balc S, Asl N, Eren E. Boron Oxide Production Kinetics Using Boric Acid as Raw Material. Am Chem Soc. 2012;51:11091–6.
37. Joos JJ, Seijo L, Barandiarán Z. Direct Evidence of Intervalence Charge-Transfer States of Eu-Doped Luminescent Materials. J Phys Chem Lett [Internet]. 2019 Apr 4;10(7):1581–6. Available from: https://doi.org/10.1021/acs.jpclett.9b00342
38. Zheng J, Ying L, Cheng Q, Guo Z, Cai L, Lu Y, et al. Blue-emitting SrB_2O_4:Eu^{2+} phosphor with high color purity for near-UV white light-emitting diodes. Mater Res Bull [Internet]. 2015;64:51–4. Available from: http://dx.doi.org/10.1016/j.materresbull.2014.12.051
39. Novoselova A V., Khokhlov VA, Shishkin VY. Redox potentials of samarium and europium in molten cesium chloride. Russ J Appl Chem. 2001;74(10):1672–7.
40. Anh NDQ, Le PX, Lee HY. Effect of red-emitting SrB_8O_{13}:Sm^{2+} phosphor on the color rendering property of white LEDs. Optoelectron Adv Mater – RAPID Commun. 2018;12(3):158–63.
41. Hao Zhang, Wen-Dan Cheng, Fa-Kun Zheng J-TC. Synthesis and Electronic Structures and Linear Optics of Solid State Compound SrB_2O_4. Chinese J Chem. 2010;19(7):641–6.
42. Demyanyshyn NM, Buryy O, Mytsyk BG, Andrushchak AS. Optimizing of the piezo-optic interaction geometry in SrB_4O_7 crystals. Opt Appl. 2016;3(August 2017):447–59.

43. Zheng T, Lis S. Huge enhancement of Sm^{2+} emission via Eu^{2+} energy transfer in a SrB_4O_7 pressure sensor. J Mater Chem C. 2020;4810–7.
44. Neefjes I, Joos JJ, Barandiarán Z, Seijo L. Mixed-Valence Lanthanide-Activated Phosphors: Invariance of the Intervalence Charge Transfer (IVCT) Absorption Onset across the Series. J Phys Chem C. 2020;124(4):2619–26.
45. Balaram V. Rare earth elements: A review of applications, occurrence, exploration, analysis, recycling, and environmental impact. Geosci Front [Internet]. 2019;10(4):1285–303. Available from: https://doi.org/10.1016/j.gsf.2018.12.005

For Table of Contents Use Only

Making Eu^{2+} and Sm^{2+} doped borates fit for solar energy applications

L.J.B. Erasmus, P.F. Smet, R.E. Kroon, D. Poelman, J.J. Terblans, J.J. Joos, D. Van der Heggen, H.C. Swart

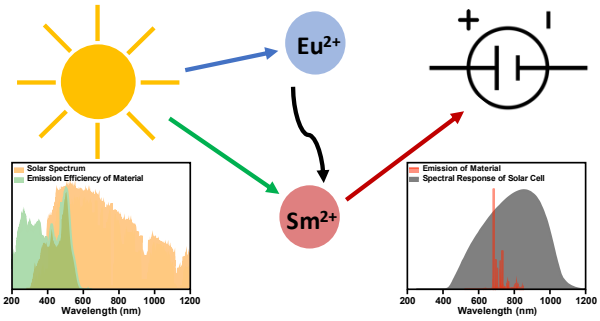

The phosphor material absorbs the solar radiation. This energy is transferred, downshifted, and emitted in the near-infrared region. A solar cell can be used to convert this radiation to energy.